Optically Modulated Fluorophores for Selective Fluorescence Signal Recovery

ARTICLE *in* JOURNAL OF THE AMERICAN CHEMICAL SOCIETY · MAY 2009

Impact Factor: 12.11 · DOI: 10.1021/ja809785s · Source: PubMed

7 AUTHORS, INCLUDING:

Dulal Senapati
Saha Institute of Nuclear Physics
52 PUBLICATIONS **2,220** CITATIONS
SEE PROFILE

Tom Vosch
University of Copenhagen
100 PUBLICATIONS **3,812** CITATIONS
SEE PROFILE

Published in final edited form as:
J Am Chem Soc. 2009 April 8; 131(13): 4619–4621. doi:10.1021/ja809785s.

Optically Modulated Fluorophores for Selective Fluorescence Signal Recovery

Chris I. Richards, **Jung-Cheng Hsiang**, **Dulal Senapati**, **Sandeep Patel**, **Junhua Yu**, **Tom Vosch**, and **Robert M. Dickson***
School of Chemistry and Biochemistry and Petit Institute for Biosciences and Bioengineering, Georgia Institute of Technology Atlanta, GA 30332-0400

Abstract

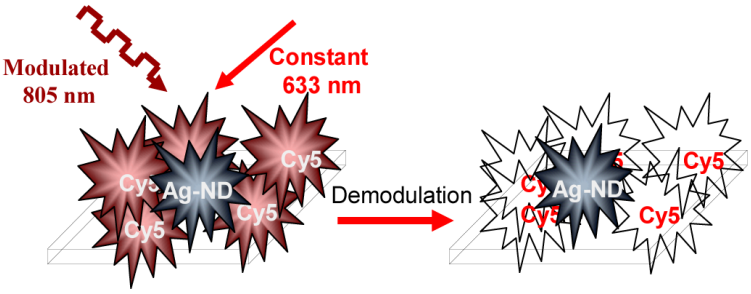

Fluorescence imaging in biological sciences is hindered by significant depth-dependent signal attenuation and high fluorescent backgrounds. We have developed optically modulated near-IR-emitting few-atom Ag nanodots that are selectively and dynamically photobrightened upon simultaneous excitation with a secondary laser enabling high sensitivity image extraction to reveal only the demodulated fluorophores. Image demodulation is demonstrated in high background environments to extract weak signals from completely obscuring background emission.

Discriminating weak signals on large backgrounds confounds many fluorescence-based detection,[1-3] dynamics,[4,5] and structural applications.[6,7] Although fluorescence contrast is readily adaptable to both medical and biological imaging, sensitivity in deep tissue and low copy number protein intracellular imaging present significant challenges. While great advances have been made,[4,5,8] available fluorophores too often access photostabilityand emission rate-impairing photoinduced dark states, thereby limiting interpretations.[9-11] Controlled photoswitching to high energy-recoverable, thermally stable, but non-fluorescent isomers has, however, been advantageously employed in the development of high resolution optical serial localization methods,[6,7,12-14] and in stochastic switching-based optical lock-in detection (OLID) schemes.[15,16] Here we report dynamic photobrightening of fluorophores with photoaccessible, but thermally *metastable* dark states that naturally decay on the 30 μs timeframe. Under simultaneous near IR illumination, these metastable dark states are rapidly optically depopulated to directly and specifically modulate fluorescence at any externally applied frequency. Simultaneous demodulation of the entire epifluorescence image (i.e. digital

*. Email: dickson@chemistry.gatech.edu.

Supporting Information Available. Experimental methods, autocorrelations of single molecules with 1 and 2 laser excitation, and pixel intensity vs time with resulting Fourier transforms for single molecule and ensemble demodulation. This information is available free of charge via the Internet at http://pubs.acs.org/.

signal processing-based lock-in detection for all pixels in parallel), specifically extracts weak ensemble and even single molecule fluorescence from high backgrounds.

Most photoswitching occurs through excited state processes that stochastically trap a non-fluorescent isomer in a thermally stable configuration. Many applications of sequentially applied, high-energy secondary excitation that stochastically recovers the original fluorescent state have been developed.[17,18] Unfortunately, the high-energy secondary beam required for switching simultaneously excites other emitters, generating significant additional background fluorescence unless applied when not imaging the sample. Additionally, switching is laser intensity dependent, forcing a compromise between bleaching and switching time to begin to approach biologically relevant timescales. Conversely, bulk fluorescence enhancement of organic dyes has been achieved via longer-wavelength, but much lower efficiency, optically induced reverse intersystem crossing.[19]Although potentially free of secondary laser-induced additional background, such studies suffer from triplet reactivity, photoinstability, and exceedingly high, biologically incompatible secondary cw laser intensities (>MW/cm^2).[19] In contrast, ssDNA-encapsulated few-atom Ag nanodot-based fluorophores have all the necessary components in place for such signal enhancements with vastly improved photostability and much lower incident intensities.[20-22] When encapsulated in ssDNA, nanoclusters or "nanodots" exhibit extremely bright fluorescence and excellent photophysics, yielding several-fold brighter and >10-fold more photostable emission than obtainable from Cy3 or Cy5, while displaying only a single dark state residence time of $\sim 30\ \mu\text{sec}$, that itself shortens with increased primary excitation intensity.[22] In contrast to the alternating illumination of two high energy wavelengths (relative to detected fluorescence) and the internal standard to measure the demodulation waveform as performed in OLID schemes, co-illumination with an intensity-modulated, long-wavelength secondary laser dynamically photobrightens higher energy nanodot emission through dark state elimination where the level of photbrightening is linearly dependent on the secondary laser intensity (see Supplemental Information fig 3S). This approach enables direct, non-interfering, fluorescence modulation to uniquely and specifically detect bright Ag nanodot fluorescence buried within high backgrounds.

Aqueous solutions of few-atom Ag nanodots encapsulated in ssDNA 5′-CCCTAACTCCCC-3,[21] yield spectrally pure, bright 710nm emitters, slightly blue shifted in excitation, but indistinguishable in size (~2.5nm hydrodynamic radius, resulting mostly from the ssDNA scaffold)from that reported previously.[22,23] Intensity-dependent nanodot excitation at 633nm revealed that not only on, but also off times, albeit at a reduced rate, decrease with increasing excitation intensity. Introduction of a non-background producing secondary laser (805nm) removes the dark state-induced premature saturation (Fig. 1a), producing up to 3-fold increases in fluorescence brightness per molecule vs that with primary 633nm excitation alone. Fluorescence enhancement with such low energy and intensity secondary excitation has not been reported with organic dyes.

For detailed analysis of fluorescent enhancement, nanodots were dispersed in poly(vinyl alcohol) (PVA) and excited at 633nm (1.2kW/cm^2). Simultaneous excitation with tunable cw secondary laser illumination yields significant enhancement of the ~710-nm emission across the entire excitation range with an excitation maximum near 775nm (Figure 1b). This excitation spectrum also appears quite similar to the absorption of anionic cytosine,[24,25] which is also readily optically depopulated with long-wavelength excitation. In order to minimize overlap with the higher energy collected fluorescence while yielding significant enhancement, 805nm secondary excitation with laser line filtering was utilized for the majority of experiments. While typical samples composed of a few molecules in the laser focus under 1.6kW/cm^2 633nm excitation easily yield ~60,000 detected photons per second (Figures 2a-c), simultaneous optically chopped (10, 100 or 1000 Hz, corresponding to Fig 2a, 2b, and 2c, respectively) illumination at 805nm dynamically modulates the emission rate, perfectly in phase with the

secondary laser modulation. The lower emissive intensity corresponds to 633 nm excitation alone and the higher levels occur only with dual laser illumination (Figure 2a-c). Fourier transforms of the resulting time traces reveal the original laser modulation frequency in each case (Figure 2d). This dynamic photobrighting is in stark contrast to OLID[15,16] and other static photoswitching[6,7,16-18] as emission is dynamically cycled between bright and brighter states, precisely at and in phase with the externally applied modulation frequency, without increasing background. The brighter level is achieved as long as the fluorophores are co-illuminated with the non-background-generating secondary laser. In contrast, photoswitches exhibit stochastic on and off times and need alternating illumination with primary and secondary light, both of which are higher energy than the collected fluorescence, thereby preculding external dynamic control of modulation cycles.[15,16] Demodulation of nanodot emission is readily performed at any imposed modulation frequency to uniquely and specifically recover nanodot fluorescence from (unmodulated) background with greatly reduced noise.

Although direct nanodot excitation at 633nm gives strong emission, the non-background-generating modulation of 700-800nm Ag nanodot emission enables extremely weak signals to be extracted from a much brighter background. As Cy5 has essentially indistinguishable emission from that of our Ag nanodots, we imaged nanodot emission localized in a thin PVA film through a high concentration solution of Cy5. With only 633nm excitation focused on the nanodot/PVA sample, >60,000 counts/pixel are observed on the ccd camera, primarily from outof-focus Cy5 emission (Figure 3a). Introduction of the same diameter 805nm laser also focused on the PVA film increased intensity on the brightest pixel by only a few percent, yet through chopping the 805nm laser, coupled with 10-fold faster synchronous wide-field imaging and simultaneous demodulation of every pixel signal in parallel (whole image demodulation), only the signal from the much lower concentration Ag nanodots is observed, and with very high contrast (Fig. 3b). The recovered image is roughly the same size (5 pixels FWHM) as the 633nm and 805 nm laser spot sizes on the PVA film, demonstrating excellent rejection of unmodulated Cy5 emission. The demodulated image results only from that area of the Ag nanocluster PVA film co-illuminated with the 805 nm laser.

The same synthetic procedure also yields photophysically indistinguishable Ag nanodots in 5′-biotinylated oligos of the same sequence. Low-density cell surface biotinylation followed by fixation and labeling with avidin, enables cell surfaces to be sparsely labeled with 710nm-emitting Ag nanodots. Highly localized, small, and sometimes blinking signals suggestive of individual molecules are readily observed, but on top of significant autofluorescence (Fig 4a). Wide field epifluorescent imaging and modulation were performed with overlapped, defocused primary and secondary laser excitation. Secondary excitation (805nm) was chopped at 1 Hz, and emission (710nm) imaged with synchronous 10-fold faster CCD detection. The modulation frequency is readily apparent in the Fourier transform of any given pixel intensity trajectory (Fig 4a inset), and clearly shows that modulation enables detection away from the lower frequency noise present in fluorescence imaging. Demodulation at the chopping frequency directly yields images with greatly improved signal/noise as (unmodulated) autofluorescent background is removed after as few as three modulation cycles (Fig 4b). In order to create a higher background environment, Cy5 solution was added to the same sample and imaged in an identical manner. Imaging through bright Cy5 solution obscures single nanodot signals (Fig 4c), but the modulation frequency is still readily apparent in the Fourier transform (Fig 4c inset). Even in the presence of bright inhomogeneous background fluorescence, demodulation again recovers the nanodot images (Fig 4d), suggesting single nanodot sensitivity on fixed cell surfaces.

Although we readily observe single molecule-suggestive signals after whole-image demodulation of nanodot fluorescence (e.g. supporting information fig 4S), verification of single nanodot sensitivity in such high background samples is challenging. Therefore, separate

samples of single nanodots (~500pM) diluted and spun in PVA and of 200nM Cy5 similarly diluted and spun in PVA were prepared and separately imaged under identical modulation and detection conditions. Films containing only Ag nanodots at this concentration yield well-resolved individual molecules exhibiting clear dipole emission patterns when slightly defocused[26,27] indicating single molecule observation. Separately imaged Cy5 samples only yield bright homogeneous background. The Cy5 background and Ag nanodot dipole emission data sets were added and the resulting ccd images (Fig. 5a) show that the dipole pattern is completely obscured by the background. Subsequent demodulation readily recovers the original dipole emission patterns, indicating true single molecule signal extraction from high background (Fig 5b), and great promise for intracellular single molecule imaging.

These unique biocompatible nanomaterials not only enable extremely high sustainable count rates through optically induced depopulation of a photoaccessed dark state, but the fast response time enables long-wavelength, high frequency modulation of dark state residence, thereby dynamically increasing fluorescence intensity. Such near IR modulation of these red-near IR emitters provides a unique digital signal processing-based method of extracting weak signals within extremely high background images, opening a significant number of single molecule and potentially bulk medical imaging applications.

Supplementary Material

Refer to Web version on PubMed Central for supplementary material.

Acknowledgement

RMD gratefully acknowledges financial support from NIH R01-GM086195 and Invitrogen. CIR acknowledges NIH NRSA F31EB008324 support, and TV acknowledges an FWO fellowship.

References

(1). Lim, Y. Taik; Kim, S.; Nakayama, A.; Stott, NE.; Bawendi, MG.; Frangioni, JV. Molecular Imaging 2003;2:50–64. [PubMed: 12926237]

(2). Tokunaga M, Imamoto N, Sakata-Sogawa K. Nat. Methods 2008;5:455–455.

(3). Sako Y, Minoghchi S, Yanagida T. Nat. Cell Biol 2000;2:168–172. [PubMed: 10707088]

(4). Kural C, Kim H, Syed S, Goshima G, Gelfand VI, Selvin PR. Science 2005;308:1469–1472. [PubMed: 15817813]

(5). Elf J, Li GW, Xie XS. Science 2007;316:1191–1194. [PubMed: 17525339]

(6). Bates M, Huang B, Dempsey GT, Zhuang X. Science 2007;317:1749–1753. [PubMed: 17702910]

(7). Betzig E, Patterson GH, Sougrat R, Lindwasser OW, Olenych S, Bonifacino JS, Davidson MW, Lippincott-Schwartz J, Hess HF. Science 2006;313:1642–1645. [PubMed: 16902090]

(8). Myong S, Bruno MM, Pyle AM, Ha T. Science 2007;317:513–516. [PubMed: 17656723]

(9). Hoogenboom JP, van Dijk E, Hernando J, van Hulst NF, Garcia-Parajo MF. Phys. Rev. Lett 2005;95:097401. [PubMed: 16197247]

(10). Schmidt T, Kubitscheck U, Rohler D, Nienhaus U. Single Molecules 2002;3:327.

(11). Bates M, Blosser TR, Zhuang XW. Phys. Rev. Lett 2005;94:108101. [PubMed: 15783528]

(12). Hu D, Tian Z, Wu W, Wan W, Li ADQ. J. Am. Chem. Soc 2008;130:15279–15281. [PubMed: 18939833]

(13). Steinhauer C, Forthmann C, Vogelsang J, Tinnefeld P. J. Am. Chem. Soc 2008;130:16840–16841. [PubMed: 19053449]

(14). Dedecker P, Hotta J.-i. Flors C, Sliwa M, Uji-i H, Roeffaers MBJ, Ando R, Mizuno H, Miyawaki A, Hofkens J. J. Am. Chem. Soc 2007;129:16132–16141. [PubMed: 18047340]

(15). Mao S, Benninger RKP, Yan YL, Petchprayoon C, Jackson D, Easley CJ, Piston DW, Marriott G. Biophys. J 2008;94:4515–4524. [PubMed: 18281383]

(16). Marriott G, Mao S, Sakata T, Ran J, Jackson DK, Petchprayoon C, Gomez TJ, Warp E, Tulyathan O, Aaron HL, Isacoff EY, Yan Y. Proc. Natl. Acad. Sci. U. S. A 2008;105:17789–17794. [PubMed: 19004775]

(17). Hess ST, Girirajan TPK, Mason MD. Biophys. J 2006;91:4258–4272. [PubMed: 16980368]

(18). Biteen, Julie S.; T., MA.; Tselentis, Nicole K.; Bowman, Grant R.; Shapiro, Lucy; Moerner, WE. Nature Methods 2008;5:947–949. [PubMed: 18794860]

(19). Ringemann C, Schonle A, Giske A, von Middendorff C, Hell SW, Eggeling C. ChemPhysChem 2008;9:612–624. [PubMed: 18324718]

(20). Junhua, Yu; S., C.; Dickson, Robert M. Angewandte Chemie International Edition 2009;48:318–320.

(21). Richards CI, Choi S, Hsiang JC, Antoku Y, Vosch T, Bongiorno A, Tzeng YL, Dickson RM. J. Am. Chem. Soc 2008;130:5038–5039. [PubMed: 18345630]

(22). Vosch T, Antoku Y, Hsiang JC, Richards CI, Gonzalez JI, Dickson RM. Proc. Natl. Acad. Sci. U. S. A 2007;104:12616–12621. [PubMed: 17519337]

(23). Petty JT, Zheng J, Dickson RM. J. Amer. Chem. Soc 2004;126:5207–5212. [PubMed: 15099104]

(24). Raytchev M, Mayer E, Amann N, Wagenknecht HA, Fiebig T. ChemPhysChem 2004;5:706–712. [PubMed: 15179723]

(25). Schiedt J, Weinkauf R, Neumark DM, Schlag EW. Chem. Phys 1998;239:511–524.

(26). Bartko AP, Dickson RM. J. Phys. Chem. B 1999;103:11237–11241.

(27). Hassey R, Swain EJ, Hammer NI, Venkataraman D, Barnes MD. Science 2006;314:1437–1439. [PubMed: 17082419]

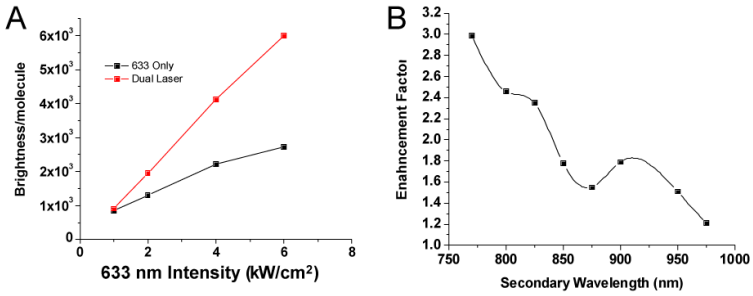

Figure 1.

A. Brightness per Ag nanodot under single laser (633nm, black) and dual laser (633nm + 805nm, red), as determined by fluorescence correlation spectroscopy, FCS. Excitation becomes prematurely saturated as the 633 nm excitation intensity increases. Simultaneous 805 nm excitation (8 kW/cm^2) recovers the linearity between excitation and 710-nm emission. B. Excitation scan of the secondary laser-based enhancement (4kW/cm^2) relative to single laser excitation (633nm 1.2 kW/cm^2).

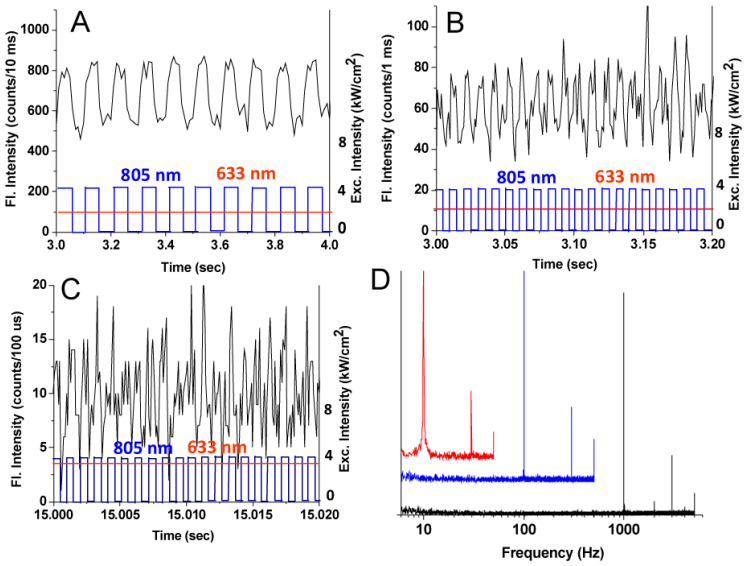

Figure 2.

PVA immobilized Ag nanodot emission collected with an APD in single photon counting mode with constant 633 nm excitation and 805 nm excitation modulated at 10 Hz (A), 100 Hz (B), and 1 kHz (C) with the respective Fourier transforms red, blue, and green with each binned an order of magnitude faster than the modulation. The externally imposed 805-nm laser modulation results in the dynamic modulation of the fluorescence from the lowemissive state to the high emissive state, with complete control down to short time regimes limited only by fluorophore brightness due to the necessity of multiple photons per bin time. With 1 kHz modulation the sample was cycled ~16,000 times with no decay in fluorescence signal.

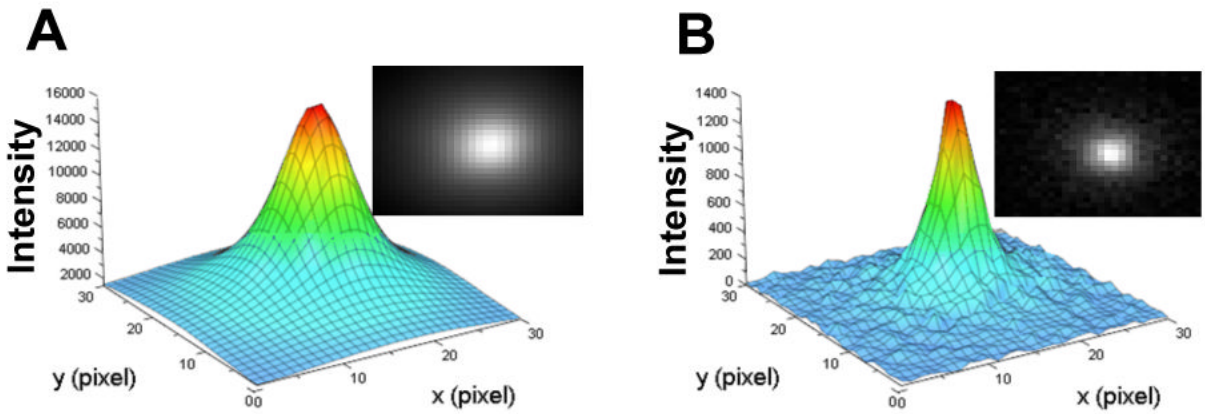

Figure 3.

Ag nanodots imaged (60x, 1.2NA, AndoriXon EMCCD, 16μm pixels) through high concentration Cy5 solution with constant defocused 633 nm-excitation (3 kW/cm^2) and optically chopped and focused 805 nm-excitation (2 kW/cm^2). A. 3-D plot of a typical raw 10ms-exposure ccd frame. (Inset) raw 2-D ccd image. B. 3-D plot of the demodulated signal with 1 sec time constant, exclusively recovering the much weaker (2% of total at brightest pixel) Ag nanodot signal. (inset) 2-D image of same 10ms frame.. Secondary laser was chopped at 10Hz, images were synchronized to the modulation, and collected at 100Hz for 10 seconds. The recovered image is roughly the same size (5 pixels FWHM) as the 805 nm laser spot size, demonstrating the background elimination and demodulated nanodot signal recovery.

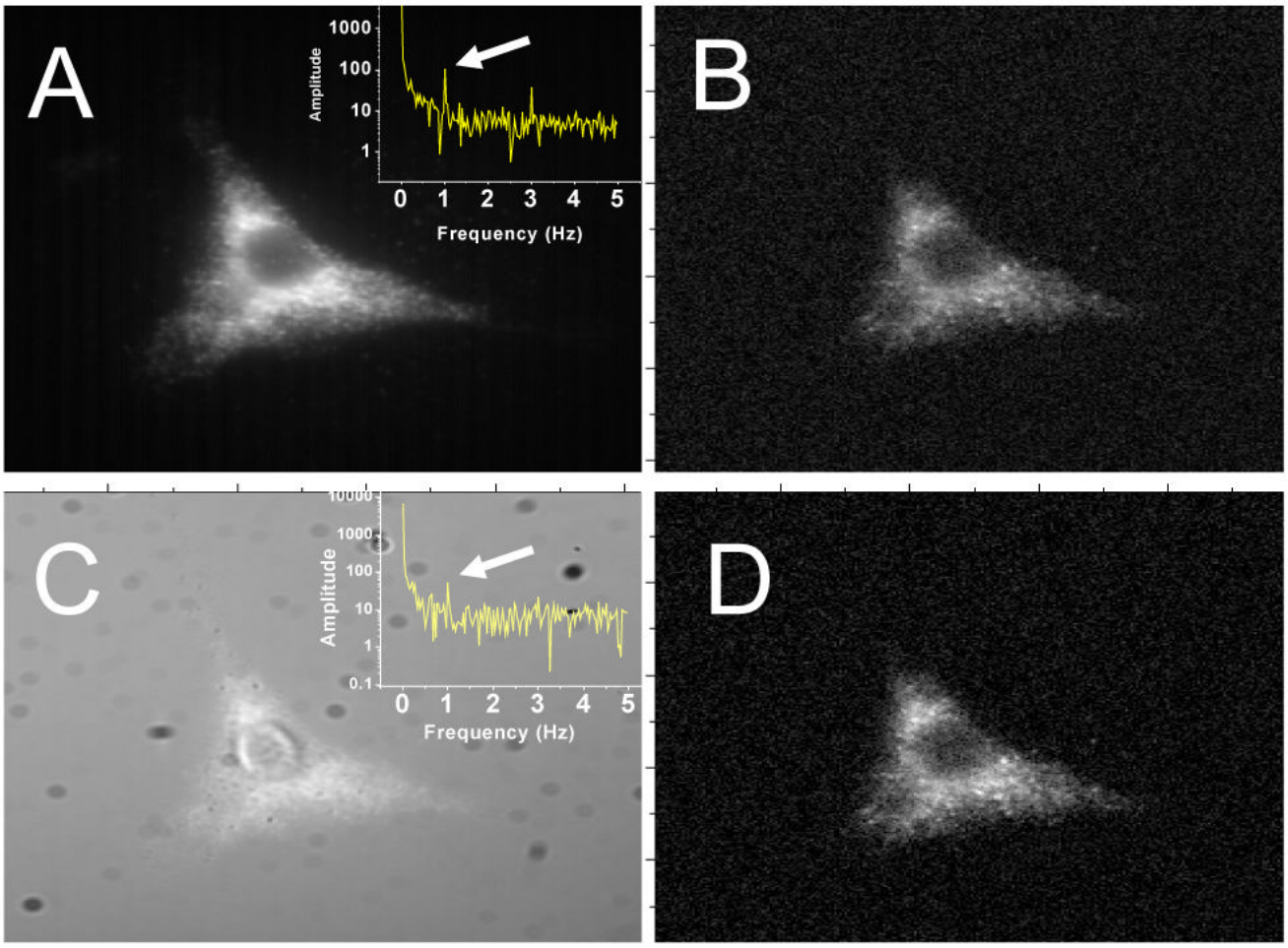

Figure 4.

A. Typical dual-laser CCD image of biotinylated NIH 3T3 cells, surface-labeled with avidin and biotinylated Ag nanodots. Secondary laser modulates the fluorescence at every pixel simultaneously. The Fourier transform of a typical pixel intensity vs. time is shown in the inset. B. Autofluorescence is removed from the recovered cell image after demodulation at the modulation frequency (indicated by the arrow in the inset to (a)) using only 3 modulation cycles. C. The same cell with high concentration Cy5 added to simulate very high autofluorescent background. The modulation frequency remains readily apparent in the Fourier transform of a typical pixel intensity vs. time (inset). D. Demodulated image (30 modulation cycles) showing the near complete elimination of the Cy5 and autofluorescent background signals leaving only the distinct signal of the Ag nanodots.

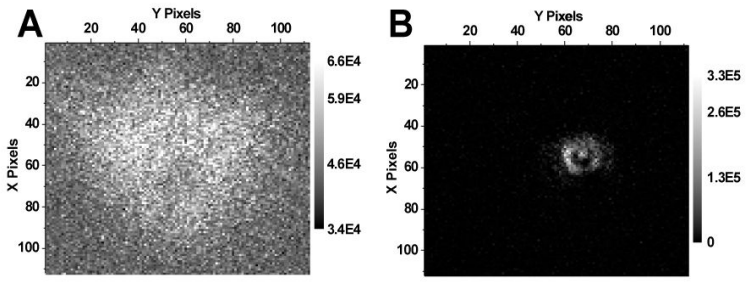

Figure 5.

A. Cy 5 (200 nM) and 710-nm-emitting Ag nanodots (~500 pM) in a PVA film imaged (1.4NA, 150x total magnification, AndoriXon (front illuminated), 7.8mM pixels, 40 Hz) under constant 633 nm excitation (800 W/cm^2) and simultaneous 805 nm excitation (6 kW/cm^2) optically chopped at 4 Hz. A. Representative 25msec frame of the combined signal from separately imaging Cy 5 (200 nM solution) in PVA and an individual Ag nanodot (defocused to show a single molecule-characteristic dipole emission pattern) also in PVA. Excitation and imaging was performed identically for each with constant 633 nm excitation (2 kW/cm^2) and 805 nm excitation (6 kW/cm^2) chopped at 4 Hz, with synchronous 40 Hz ccd detection. B. The demodulated image (10 second time constant) clearly shows the otherwise unobservable single nanodot dipole emission pattern without the large background.